Applied Catalysis B: Environmental 150–151 (2014) 249–256

Contents lists available at ScienceDirect

Applied Catalysis B: Environmental

journal homepage: www.elsevier.com/locate/apcatb

Surface and electrochemical characterisation of a Pt-Cu/C nano-structured electrocatalyst, prepared by galvanic displacement

Bart Geboes[a,b,*], Ioanna Mintsouli[d], Benny Wouters[a], Jenia Georgieva[c], Alexandros Kakaroglou[a], Sotiris Sotiropoulos[d], Eugenia Valova[c], Stephan Armyanov[c], Annick Hubin[a], Tom Breugelmans[a,b]

[a] Vrije Universiteit Brussel, Research Group Electrochemical and Surface Engineering, Pleinlaan 2, 1050 Brussels, Belgium
[b] University of Antwerp, Applied Engineering – Chemistry, Salesianenlaan 30, 2660 Hoboken, Belgium
[c] Bulgarian Academy of Sciences, Rotislaw Kaichew Insitute of Physical Chemistry, Acad. G. Bonchev Str. bl. 11, Sofia 1113, Bulgaria
[d] Aristotle University of Thessaloniki, Department of Chemistry, University Campus, Thessaloniki 54124, Greece

ARTICLE INFO

Article history:
Received 21 August 2013
Received in revised form 6 December 2013
Accepted 13 December 2013
Available online 22 December 2013

Keywords:
Electrocatalyst
ORR
Nanoparticle
Transmetalation
Galvanic replacement

ABSTRACT

A two-step procedure at room temperature was applied to prepare a bimetallic Pt-Cu carbon-supported catalyst (Pt-Cu/C). First the chemical reduction of Cu ions by sodium borohydride in the presence of Vulcan XC72R carbon powder is performed. Second, the partial galvanic replacement of Cu particle layers by Pt is achieved upon immersion in a chloroplatinate solution. The characterisation of the Pt-Cu/C catalyst by XRD and XPS proves the formation of Pt-Cu alloying. The electrochemical active surface area (EASA) is determined for the Pt-Cu/C transmetalation catalyst as well as for a commercial Pt/C catalyst from the Alfa Aesar HiSpec® product line. The resemblance in surface voltammetry is an indication for a Pt rich shell. The catalytic activity towards the oxygen reduction reaction for both catalysts is evaluated by using linear sweep voltammetry (LSV) in combination with a rotating disc electrode. Koutechý–Levich analysis shows that the Pt-Cu/C catalyst has a higher catalytic activity towards the oxygen reduction reaction (ORR) at 0.8 V and 0.85 V vs RHE compared to the tested commercial catalyst. The activity increase is attributed to a "ligand effect"-modification of the core metal on the Pt shell.

1. Introduction

Polymer electrolyte membrane fuel cells (PEMFC) provide a promising link in the future sustainable energy cycle. Zero emission vehicles as well as stationary fuel cell systems are already in the development stage. The major disadvantage today is the higher capital cost compared to conventional electricity production methods [1,2]. The performance of the cathode electrocatalyst in PEMFC's is of paramount importance due to the sluggish electroreduction of molecular oxygen to water at the cathode side. The fairly strong Pt-O surface bond is believed to lie at the basis of the slow oxygen reduction reaction (ORR) kinetics [3]. Unsupported or carbon-supported pure Pt materials are the most widely used cathode electrocatalysts during the last decades [4]. Alternative catalyst materials could dramatically decrease the capital cost through an increase in catalytic activity—resulting in higher fuel cell (FC) efficiency—or through a lower Pt content. Two strategies are deployed in the search for more active ORR electrocatalysts; on one hand lowering the Pt amount in Pt-M alloys [5–8] and on the other hand the search towards non-Pt catalyst concepts [9–11].

Over the years several Pt-M alloy catalysts have shown to significantly increase activity towards ORR due to the alloying effect [12]. Amongst them, Pt-Pd and Pt-Co alloy catalysts were extensively studied [13,14]. The alloying augments the surface area-based activity as well as the Pt mass-based activity. Especially from an economic point of view the latter provides a good basis to benchmark FC electrocatalysts. Where the surface area based activity significantly increases, the Pt mass based activity undergoes only a rather small attenuation leading to an almost equally expensive catalyst. The solution to this problem is brought by controlling the nanoparticle morphology to form core–shell structures. As little as a few monolayers of the shell metal can be deposited on an alloyed or single metal core. Consequently the mass based activity is drastically increased.

High temperature annealing is frequently applied in order to segregate Pt-M alloyed nanoparticles into a core–shell structure. Despite the increase in specific activity, particle sintering causes a dramatic decrease in electrochemical surface area (ECSA) [15,16]. Wei et al. reported the electrodeposition of Cu nanoparticles on porous carbon electrodes [17]. Even though this technique enables

* Corresponding author at: University of Antwerp, Applied Engineering - Chemistry, Salesianenlaan 30, 2660 Hoboken, Belgium. Tel.: +32 32051845; fax: +32 26293200.
E-mail address: bart.geboes@uantwerpen.be (B. Geboes).

0926-3373/$ – see front matter © 2013 Elsevier B.V. All rights reserved.
http://dx.doi.org/10.1016/j.apcatb.2013.12.020

an effective use of noble metal catalysts due to exclusive deposition on accessible electrode regions, minimum particle sizes remain 20–70 nm. Electroless methods on the other hand have the advantage of creating nanoparticles in the 2–5 nm diameter range. Fine tuning the nanoparticle morphology to create a core–shell structure can be done by electrochemical [4] or chemical [18] leaching of the core metal or through the deposition of an additional metal layer [19].

An alternative method for the preparation of multimetallic catalysts has been developed, based on the spontaneous replacement of an initially deposited less noble metal by a more noble one, a process often termed galvanic replacement or transmetalation [20,21]. It was first applied by Adzic and co-workers [22–25] for the complete replacement of Cu UPD monolayers by Pt, Pd or Ag and then by a series of noble metals or their mixtures. Kokkidinis and co-workers [26,27] applied the technique to the partial replacement of electrodeposited Cu and Pb polylayers by Pt (resulting in Pt shell—Cu or Pb core particles). This approach has been recently further developed by Sotiropoulos and co-workers who prepared Pt-Cu, Pt-Pb, Pt-Fe, Pt-Co, and Pt-Ni binary catalysts by the transmetalation process and tested them with respect to their activity towards oxygen reduction [28,29] and hydrogen evolution [30]. This technique has been taken to the next step by preparing core–shell Pt-Cu nanoparticles on a porous carbon support [20,31,32]. The simple replacement reaction between the Cu nanoparticle catalyst and a Pt salt not only provides better control of morphology, but also presents a low cost production method for porous carbon deposited nanoparticle FC catalysts [32].

It was found recently that model Pt/Cu electrodes, prepared by the transmetalation of Cu layers on glassy carbon [30] and their particle analogues prepared from Cu particles on Vulcan XC72R carbon support [33] exhibited higher medium-term activity towards methanol oxidation. Based on these findings the aim of this work is to assess the electrocatalytic activity of Pt-Cu/C powder catalysts towards oxygen reduction reaction in comparison with a commercial Pt/C catalyst with similar Pt loading. The continuation of the two-step method as an alternative route for the preparation of practical Cu@Pt catalysts is used. Due to the ease for Cu to form oxides in neutral and basic media only few authors reported on the galvanic replacement process with Pt [34]. As a result many hiatuses still remain in the formation of the supposed core–shell structure. The obstacles of Cu@Pt nanoparticle formation will be overcome in this work through applying the two-step galvanic replacement process. Formation, properties and ORR activity of the synthesised Cu@Pt nano-structured catalyst will be evaluated. Surface characterisation techniques such as EDS, TEM an XPS will be combined with the electrochemical characterisation using linear sweep voltammetry (LSV) in combination with rotating disc electrode (RDE). Special attention will be devoted to H UPD measurements since intrinsic catalytic activity as well as the practical application of the catalyst is indicated by the electrochemical active surface area (EASA).

2. Experimental

2.1. Preparation of a Cu@Pt transmetalation catalyst [33]

The support for the catalyst is high surface area carbon black powder (Vulcan XR 72, Cabot), a typical substrate used in fuel cell environments. To activate the carbon powder it was exposed to an oxidative pretreatment, leading to an increased number of the functional groups on the surface [35]. For this purpose 0.25 g carbon black (Vulcan XC72) is treated with a 1 M sulfuric acid and 10% (w/v) ammonium persulfate solution during 24 h of magnetic stirring at room temperature. The obtained suspension is then filtered, and the precipitate is rinsed with distilled H_2O and left to dry overnight. The oxidised carbon is mechanically ground in a mortar and suspended in 90 ml water. Then a two-step catalyst preparation procedure is applied. First the carbon powder is impregnated with an ionic solution of the non-noble metal, prepared by dissolving 0.4 g $CuSO_4 \cdot 5H_2O$ (0.1 g Cu or 0.0016 g-atom of Cu; Sigma–Aldrich (ACS reagent)) in 10 ml water and adding it to the carbon suspension. Maximum copper ion adsorption on the carbon surface is ensured by magnetically stirring the preparation during a 24 h period. To reduce the adsorbed Cu(II), a 1 M NaOH solution containing 12.8 ml (0.0128 mol) of 0.1 M $NaBH_4$ is added to the suspension (an excess of reducing agent is created). The resulting suspension is stirred in an ultrasonic bath for 30 min and filtered afterwards. Second, the obtained Cu/C precipitate is left to dry in air and is then slowly added under continuous stirring to 50 ml of 10^{-2} M K_2PtCl_6 solution containing 0.1 M HCl for the electroless platinisation to occur:

$$Cu/C + PtCl_6^{2-} \rightarrow Pt\text{-}Cu/C + Cu^{2+} + Cl^- \quad (1)$$

The reaction mixture was stirred in the ultrasonic bath for another 30–45 min, filtered and left to dry in air. With this nanoparticle powder the catalyst inks were prepared and coated on the glassy carbon electrodes for further electrochemical tests. The developed Pt-Cu/C nano-structured catalyst is benchmarked to a well-known commercial Pt nanoparticle catalyst. This commercial catalyst from the Alfa Aesar HiSpec® catalyst line (product number 35849) is optimised for usage in fuel cells and is supported on a porous carbon black substrate. The chosen metal loading of this catalyst is 20 wt%, comparable to the Pt loading in the Cu@Pt catalyst.

2.2. Microscopic, spectroscopic and crystallographic characterisation

Transmission electron microscopy (TEM) was carried out using a Philips M20 TEM system. Energy Dispersive Spectroscopic (EDS) elemental analysis was performed using the utility of a JEOL JEM 6390/EDS system. X-ray Diffraction patterns of the catalyst powders were obtained using Cu anode—WL1 Kα filtered radiation (λ = 1.5406 Å) and scintillation registration with a constant scanning step $\delta(2\theta) = 0.02^\circ$, and a counting time per step of 3 s. X-ray photo electron Spectroscopy (XPS) studies were performed in a PHI model 1600 system equipped with an Omni Focus Lens III using a standard Mg Kα X-ray source at a high voltage of 15 kV, 300 W. The PHI Multipak 8 software was used for data interpretation.

2.3. Electrode preparation and electrochemical characterisation

Electrochemical experiments are done in a three-electrode electrochemical cell using a Ag/AgCl reference electrode with a Luggin capillary and a Pt wire counter electrode. A 0.5 M H_2SO_4 electrolyte solution is used. The glassy carbon working electrode (0.6 cm diameter) is coated prior to the tests with the catalyst ink, consisting of a suspension of the catalyst powder in a 50:50 water isopropanol mixture. The catalyst inks were sonicated for 2 hours to ensure a homogeneous suspension. Using a micro pipette, 5 μl of the catalyst ink is applied at the glassy carbon surface resulting in a catalyst coverage of 15 $\mu g/cm^2$. After the electrodes have dried to the air at room temperature for roughly 15 min a thin perfluorosulfonic acid (PFSA) layer—also known under the commercial name Nafion®—is applied by adding 10 μl of 5% PFSA solution in 50:50 water–alcohol solvent. This layer acts as a binder for the catalyst powder to produce mechanically stable electrodes while assuring the proton transport towards and from the active surface.

CV measurements are obtained using a Biologic VSP-300 potentiostat equipped with an analogue scan generator. The LSV measurements are performed using an Autolab PGSTAT 302F in combination with a Radiometer EDI101 rotator.

3. Results and discussion

3.1. Microscopic, spectroscopic and crystallographic characterisation

TEM micrographs of the Pt(Cu)/C catalyst are presented in Fig. 1(a). The carbon support consists of 30 nm spherical particles that are further aggregated in chain-like structures. The Pt(Cu) particles resulting from the immersion of the precursor Cu/C in a chloroplatinate solution according to Eq. (1) show a tendency to form aggregates in the 10–20 nm range. Smaller structures can be seen within these aggregates. A particle size of 3.9 nm is obtained from XRD results that will be presented later. The crystallites of the commercial Pt/C reference catalyst have a size of ca. 2 nm and appear to be well dispersed in Fig. 1(b).

EDS analysis of the Pt/C and Pt-Cu/C catalysts is shown in Table 1. The platinum contents in the commercial and transmetalation catalyst are 20 wt.% and 22.7 wt.% respectively. Taking the 2σ error into account the Pt loading of both catalysts is comparable with domination of Pt-Cu/C to the extent of ~15%. We would like to note that the atomic ratio Pt/Cu in Pt-Cu/C is 4.5:1 whereas it was 1:1 in the previous study [33], where lower quantities of the Pt chlorocomplex were used (the chloroplatinate solution was 1E−3 M in that case). The strong effect of Pt concentration in the transmetalation solution in tuning catalyst composition will be the subject of other studies. As discussed previously, there is a collapse of large Cu particles during the platinisation process as well as a further dissolution of uncovered Cu, coupled with oxygen reduction in the acidic environment.

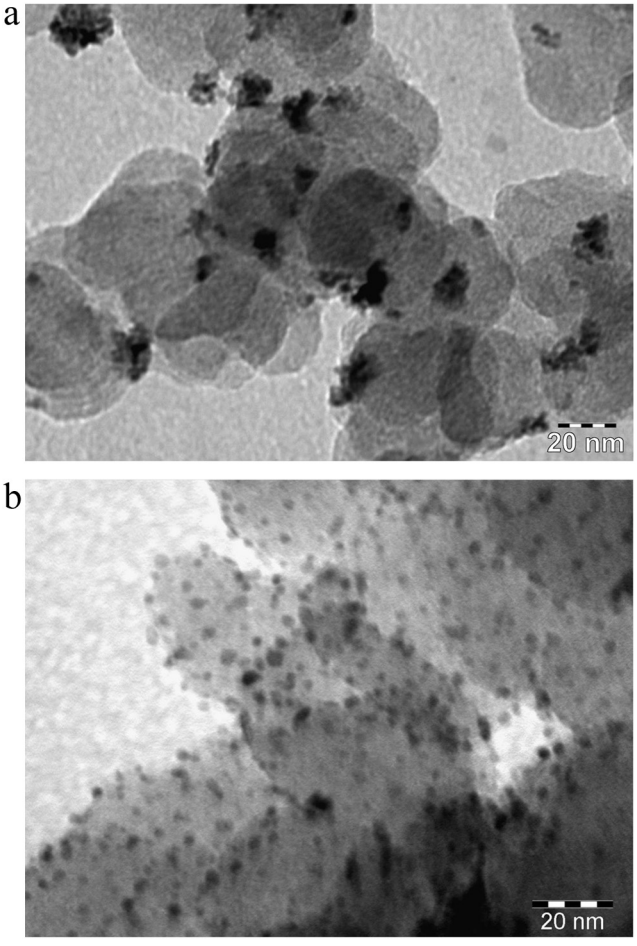

Fig. 1. (a) TEM image of *s*. Pt-Cu/C. The individual particle size is about 3–4 nm. (b) TEM image of commercial Pt/C catalyst. Particle size 1–2 nm. Both images are marked with a 20-nm scale.

Table 1
EDS element analysis of the Pt-Cu transmetalation catalyst and commercially available Pt/C catalyst

	Pt-Cu/C			Pt/C		
Element line	Weight%	Error	Atomic%	Weight%	Error	Atomic%
C K	72.7	±0.74	94.7	80.0	±0.32	98.5
Cu K	1.5	±0.26	0.4	–	–	–
O K	3.2	±0.54	3.1	–	–	–
Pt M	22.7	±0.60	1.8	20.0	±0.32	1.5
Total	100.0		100.0	100.0		

The chemical state and composition of the surface layers of the catalyst was further probed by XPS. Fig. 2 shows the XPS spectra corresponding to a region of Cu 2p peaks for the as received and after etching by Ar-sputtering during 100 s. It is hard to detect peaks in case no sputtering is applied. Taking into account BE of Cu 2p and application of Mg Kα X-ray excitation (1253.6 eV) it is possible to evaluate the electron inelastic mean free path, λ on the base of kinetic energy [36]. It is accepted that a distance about 3λ (in this case it is 2.1 nm) is able to cause the 95% attenuation of Cu 2p signal. However, it is necessary to note that it is not reasonable to expect a continuous Pt shell with uniform thickness. In addition we can expect a smooth compositional transition between the shell and the core instead of a sharp changeover.

Fig. 3 shows a region of the XPS spectrum where 4f peaks appear attributable to Pt. They are very well resolved both before as well as after sputtering. At first sight the Pt 4f peak intensity increase after sputtering contradicts the presence of a Pt rich shell. Given the Cu 2p peaks only appear after sputtering it is more likely that the increased intensity is due to the removal of the surface carbon atmospheric contamination layer of typically ca. 1 nm thickness. Opposed to [33] the Cu 3p signal should be weak enough and overlap with Pt 4f peaks. The latter should not be observable as in previous XPS results of a Pt-Cu/C catalyst with a fivefold lower Pt/Cu atomic ratio [33]. The reason is the dominating Pt 4f signal. As should be expected there are clear Pt 4f peaks in the Pt/C nanocatalyst.

The peaks on the diffraction pattern can be seen very well in Fig. 4. It is clear that they belong to a face-centered cubic (FCC) structure of the deposited Pt crystallites, although there is a shift with respect to the pure Pt peaks. They are symmetrical and there

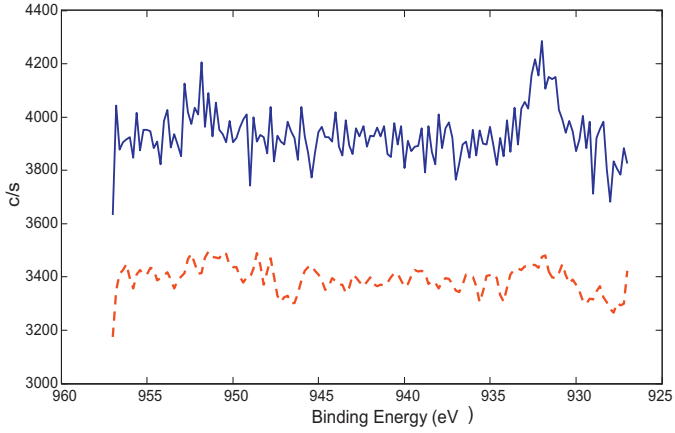

Fig. 2. XPS Cu 2p spectra of Pt-Cu/C particles prepared by chemical reduction and galvanic replacement: red (dashed) before Ar sputter-etching of the surface; blue after Ar sputter-etching of the surface. The reference BE are: Cu2p3/2 932.7 eV, Cu2p1/2 952.5 eV. (For interpretation of the references to color in this figure legend, the reader is referred to the web version of the article.)

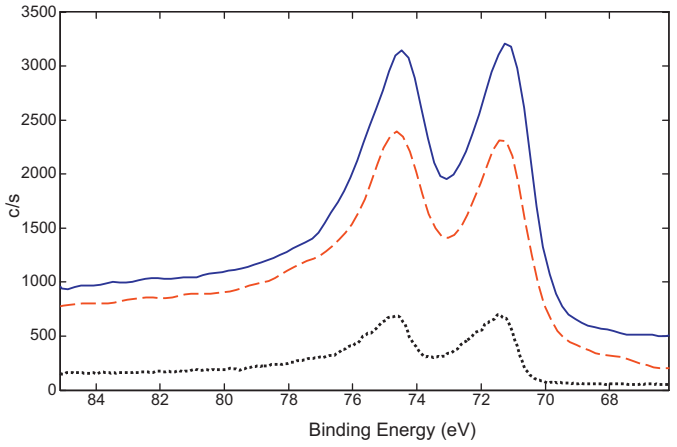

Fig. 3. XPS Pt 4f spectra of Pt/C—black (dotted line) and Pt-Cu/C particles prepared by chemical reduction and galvanic replacement: red (dashed) before Ar sputter-etching of the surface; blue after Ar sputter-etching of the surface. The reference BE are: Pt4f7/2 71.12 eV, Pt4f5/2 74.45 eV. The spectrum of Pt/C is taken using different equipment which is the reason for the difference in count numbers. (For interpretation of the references to color in this figure legend, the reader is referred to the web version of the article.)

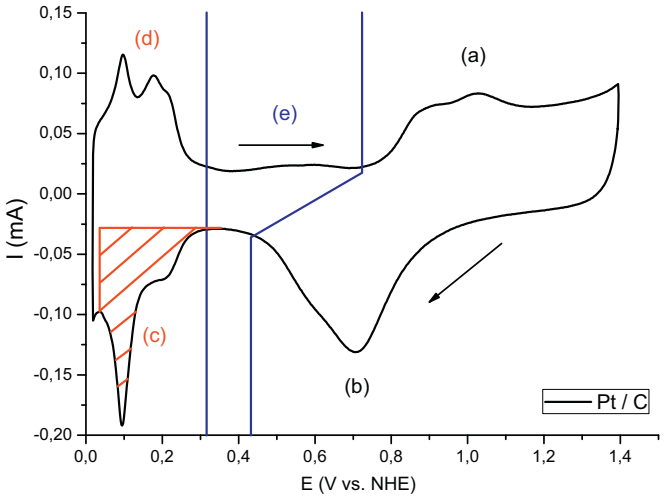

Fig. 5. Cyclic voltammogram of the hydrogen underpotential deposition on the Pt/C catalyst in a N_2 saturated electrolyte solution. Pt oxidation peaks (a) as well as a PtO reduction peak (b) can be distinguished. Additional regions are: hydrogen adsorption (c) and desorption (d) and the electrochemical double layer region (e).

is no sign of Cu lattice. The small peak at $2\theta \sim 25$ grad belongs to carbon. All peaks of Pt-Cu/C including the strongest [1 1 1] are broad, suggesting very small particle dimensions. Using the Sherrer's formula the particle size is about 3.9 nm which corresponds with the observations in TEM micrographs (Fig. 1).

The lattice parameter is determined to be 3.855 Å considering the extrapolation of the lattice parameter towards $\cos(\theta) = 0$ against$(\sqrt{(}\cos\theta))$. Presuming Vegard's law holds (linear approximation between Pt and Cu content) and using data for Pt (JCPDS 04-0802 as on the figure) and Cu (JCPDS 04-0836) it was obtained that Pt-based solid solution has been formed with composition: Pt 78 at.% and Cu 22 at.%. The ratio Pt/Cu determined from XRD is 3.5, from EDS analysis—5 and from XPS surface survey—6. A qualitative explanation in the difference between the EDS and XRD results could be that Pt and Cu are not fully alloyed. A similar type of explanation for the difference of both techniques from the findings of XPS could be that the latter is more surface sensitive. However, at a quantitative level, making this comparison besides well known specific features of each method one should keep in mind that in the case of nanoparticles there are additional peculiarities both for XPS [37] and for EDS [38] analysis. Not very often one can find similar comparisons in the literature and when they are available the discrepancies are larger.

3.2. Electrochemical characterisation

3.2.1. Electrochemical active surface area (EASA) determination

The obtained cyclic voltammogram of the Pt/C catalyst in a nitrogen saturated electrolyte solution can be seen in Fig. 5. In the cathodic scan between ca. 0.3 V and 0.4 V and in the anodic scan between 0.3 V and 0.7 V the electrochemical double layer region is visible (e). The hydrogen adsorption/desorption peak emerges in the region of 0.05–0.25 V (c/d). The main characteristic of the peak is that it has 2 well-delineated sub-peaks. The two main anodic H peaks and their cathodic counterparts are usually attributed to two different forms of adsorbed H namely, strongly

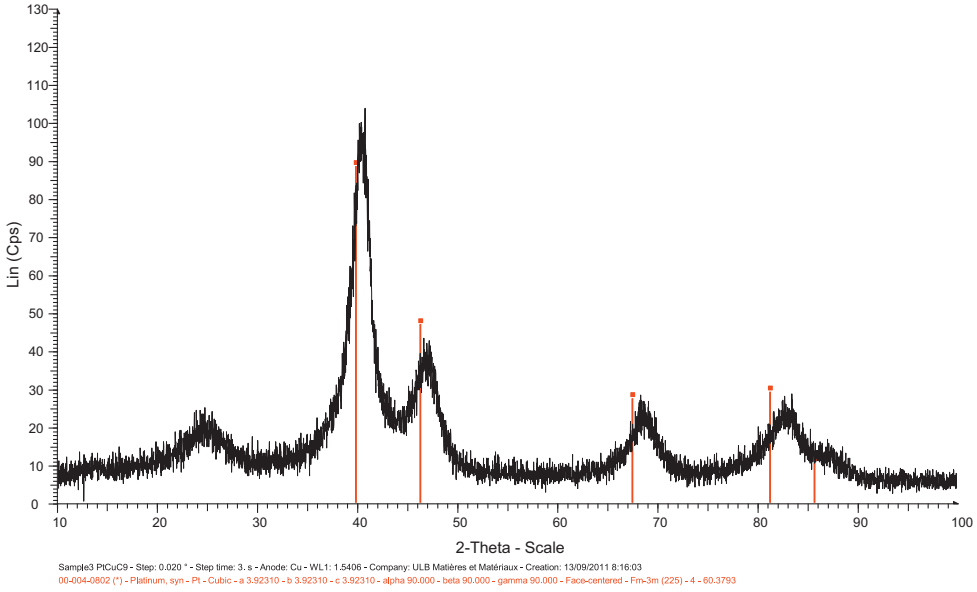

Fig. 4. XRD diffractogram of Pt-Cu/C particles prepared by chemical reduction and galvanic replacement. For XRD patterns of Vulcan XC72R C, Pt/C (ETEK) and Cu/C see [33]

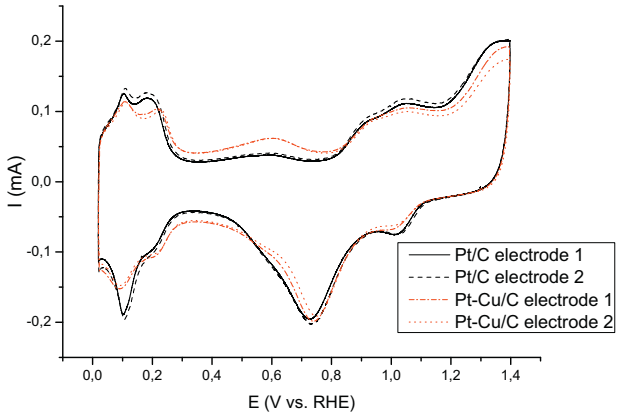

Fig. 6. Cyclic voltammograms of the hydrogen underpotential deposition on the Pt/C and Pt-Cu/C catalysts in a N_2 saturated electrolyte solution. The variation of the EASA is shown for 2 electrode applications.

and weakly bound H. The shoulder in the second anodic peak is usually attributed to the coupled bisulfate anion desorption process in the sulfuric acid electrolyte [39,40].

The hydrogen adsorption peak can be integrated to calculate the total charge passed during the adsorption process. The boundary conditions for determining the potential range of this peak are the relative maxima in the double layer region and before the onset of the hydrogen evolution (hatched area in Fig. 5). Through the weighted average coverage area of the H atoms in polycrystalline Pt, the proportionality constant of 210 $\mu C/cm^2$ is calculated [41,42]. Via this value the EASA can be calculated from the charge amount of the hydrogen adsorption peak.

$$\text{EASA}\,[\text{cm}^2\,\text{Pt/g Pt}] = \frac{Q\,[\mu\text{C/cm}^2]}{210\,[\mu\text{C/cm}^2\,\text{Pt}] \quad \text{electrode loading}\,[\text{g Pt/cm}^2]} \qquad (2)$$

The general shape of the cyclic voltammograms for the Pt-Cu/C catalyst (Fig. 6) is similar to this of the Pt/C catalyst indicating a Pt-surface response. In case of a shell containing only copper (e.g. as an underpotentially deposited, UPD, Cu monolayer), the H adsorption–desorption peaks should be completely suppressed [43,44]. In case of a uniformly alloyed catalyst shell these peaks and the associated charge should decrease (since H adsorption does not occur on Cu) resulting in much lower EASA values. At the same time, any Cu exposed to the solution should anodically be dissolved at positive potentials and this would give rise to high anodic currents, completely blurring the Pt electrochemical response.

The ink application for each catalyst is performed twice in order to investigate the variation in the structure of the porous electrode. Electrode loadings are 14.28 $\mu g/cm^2$ and 15.59 $\mu g/cm^2$ for the Pt/C and Pt-Cu/C catalysts respectively. The double layer region currents and H adsorption/desorption region more or less overlap for both coated electrodes of each catalyst. This indicates the reproducibility of the performed catalyst coating procedure. The applied amount of catalyst is comparable due to a homogeneous ink suspension and results in an equally thick porous layer. Consequently, even minute differences in EASA can be detected and corrected for in the activity measurements.

There is however a difference in the current value of the double layer region between Pt-Cu/C and Pt/C. The same can be said on the charge amount in the H adsorption/desorption region. Currents in the hydrogen adsorption region have a magnitude of ca. 0.15 mA in contrast to the 0.2 mA in the Pt/C voltammograms. Hence the calculated EASA of the Pt-Cu/C catalyst will be smaller as for Pt/C. A plausible cause is the smaller particle size of Pt/C (1–2 nm) compared to the Pt-Cu/C catalyst (3–4 nm) obtained by TEM. Another reason could be the partial blocking of the metal nanoparticles of Pt-Cu/C by the observed coagulates formation in TEM micrographs. Cu segregation towards the surface of the nanoparticles could also result in a lower measured EASA. Since none of the performed surface characterisation techniques showed evidence of this phenomenon, this is an unlikely event.

Table 2
Calculated EASA values for two consecutive electrode preparations of each examined catalyst.

	EASA (m^2 Pt/g Pt)	
	Pt-Cu/C	Pt/C
Electrode 1	34.81	40.45
Electrode 2	32.95	43.14
$\bar{x}$	33.88 ± 2.64	41.80 ± 3.81

A possible interpretation of any significant changes in H adsorption/desorption peak position upon passing from Pt to Pt-Cu could be based on a decrease of the Pt-Cu adsorption affinity as a result of a downshift of the Pt d band centre [3]. However, this should have shifted all peaks to more negative potentials (or at least, both conjugate peaks of the weakly adsorbed H—corresponding to more negative potentials). Since such a trend is not present and given the rather small changes in some of the peak positions, we are tempted to attribute these changes to differences in the underlying (high) capacitive currents and other uncertainties often encountered in the voltammetry of high surface area, carbon supported electrodes.

For both Pt-Cu/C and Pt/C catalysts the PtO reduction peak is visible in the vicinity of 0.7 V. A general difference stands out in the double layer region of the Pt-Cu/C voltammograms in relation to the Pt/C voltammograms. A small peak is observed at 0.6 V in the anodic scan direction and is attributed to the Vulcan carbon support surface electrochemistry [33]. Although this peak is also present in the Pt/C voltammograms, it is more pronounced for Pt-Cu/C. Due to larger Pt particles and aggregates there is a higher C surface available in the Pt-Cu/C catalyst. This effect can possibly be augmented due to the oxidative treatment of the C support in the nano-structured Pt-Cu/C catalyst, increasing its surface area.

The calculated EASA values (Table 2) for all four electrodes clearly indicates little variation is obtained over consecutive catalyst applications of the same type of catalyst. It can be seen that the average EASA ($33.88 \pm 2.64\ m^2$ Pt/g Pt) is smaller compared to the commercial catalyst ($41.80 \pm 3.81\ m^2$ Pt/g Pt). It should be stressed that preliminary EASA measurements are indispensable prior to catalytic activity measurements. If EASA is not taken into account, calculated current densities using the geometric surface area of the GC working electrode will deviate considerably from actual activity.

3.2.2. ORR activity

The linear sweep voltammograms in this section are all obtained at a scan rate of 5 mV/s using a rotating disc electrode. The potential is swept starting at 0.017 V vs. RHE in positive direction in order to avoid too much *H* adsorption in the lower potential region. To check the influence of possible capacitive currents a blanc sweep obtained in a nitrogen saturated electrolyte solution is performed. The ORR sweeps are on their turn obtained after saturating the electrolyte solution with oxygen during a 15-min window.

In Fig. 7 (a) the typical linear sweep voltammogram is obtained for the Pt/C catalyst at various rotation speeds. After a region with no activity between 1.4 V and 0.93 V the onset of the ORR at 0.93 V initiates the kinetic region until ca. 0.85 V. The potential–current relationship is given by the Butler–Volmer equation due to the kinetic control of the ORR. The mixed kinetic and diffusion region spans until ca. 0.6 V, where it transfers into the diffusion limited region. The measured current plateau is a result of the fixed RDE rotation rate, delivering oxygen at a constant rate.

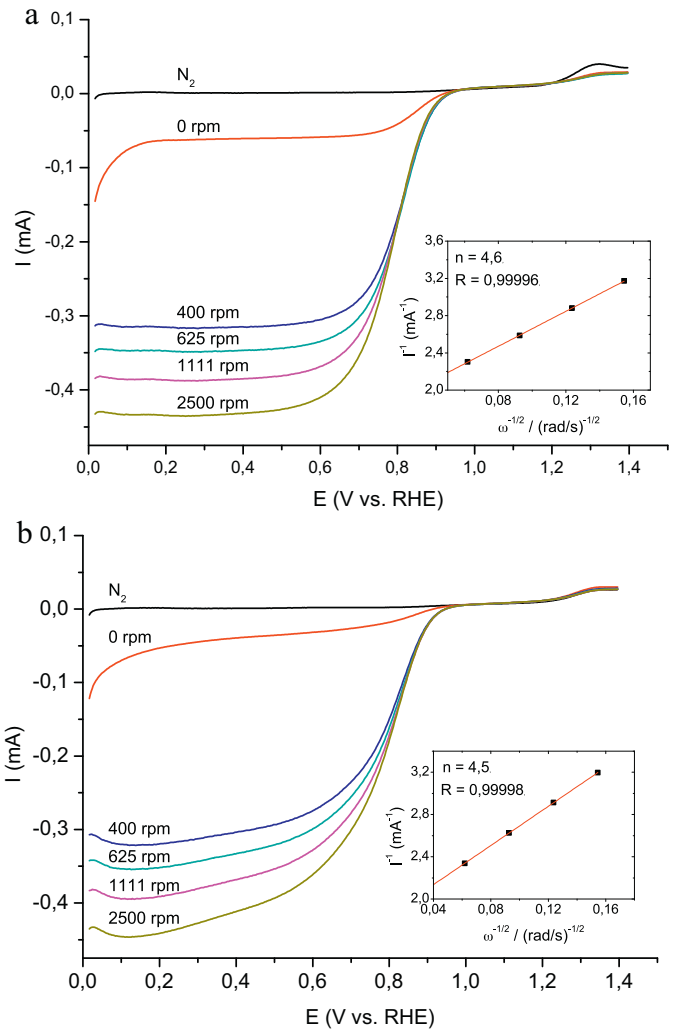

Fig. 7. Linear sweep voltammograms obtained at 5 mV/s from the porous electrodes using different RDE rotation speeds. Inset shows the Koutechý–Levich plot obtained at the diffusion plateau of Pt/C and Pt-Cu/C at 0.2 V and 0.1 V respectively.

The two consecutive electrode measurements of the Pt/C catalyst (only one is shown here) show a similar course to Fig. 7. A single well-formed reduction wave is observed in both measurements. The lack of variations is another indication for the reproducibility of the complex interface of the porous electrode containing the carbon support, metal nanoparticles and the PFSA binder. Unlike the ORR kinetics, which should not alter on the same catalyst material, the diffusional limitations could possibly be altered by a different composition and loading of the porous electrode. The conclusion that these variations are kept in a small range can be drawn from the current values of the diffusion plateau. For electrode 1 and 2 these are −0.43 mA and −0.45 mA respectively for the highest rotation speed (2500 rpm).

In the case of the Pt-Cu/C catalyst (Fig. 7(b)) the situation is somewhat different. Although the onset potential (0.95 V) and the single reduction wave of the curves are similar to the Pt/C catalyst, there is a variation in the potential range of the diffusional plateau (0.1–0.15 V). Even though a rather narrow potential range plateau is obtained at 0.12 V, the comparable number of exchanged electrons (n) from Eq. (4) indicates the reaction mechanism is not altered in respect to Pt/C. The more inclined shape of the curve in the mass transfer region of Pt-Cu/C could be attributed to differences in surface chemical steps associated with the reaction of the intermediate H_2O_2, due to differences in the electrode surface state at those potentials (as hinted by changes in the surface voltammetry of Fig. 6). Complete Pt oxide reduction during the negative potential scan seems to be completed earlier on Pt-Cu/C electrodes (Fig. 6). Since the presence of oxides is known to catalyze H_2O_2 decomposition at the surface towards O_2 which is further reduced at the electrode [45], their absence may increase H_2O_2 surface concentration which (especially at higher mass transfer rates) will be lost to the solution, resulting in lower currents.

The Koutechý–Levich plots calculated in the diffusion limited current region are shown for both catalysts as insets in Fig. 7. Calculations were done using Eq. (3), with the values of $D_{O_2} = 1.4E{-}5\ cm^2\ s^{-1}$, $\nu = 0.01\ cm^2\ s^{-1}$ and $C_{O_2} = 1.1E{-}6\ mol\ cm^{-3}$ for the diffusion coefficient, kinematic viscosity and dissolved oxygen concentration respectively in a 0.5 M H_2SO_4 solution [46].

$$\frac{1}{I} = \frac{1}{I_k} + \frac{1}{B\omega^{1/2}} \tag{3}$$

$$B = 0.62nFAD_{O_2}^{2/3}\nu^{-1/6}C_{O_2} \tag{4}$$

The calculated number of exchanged electrons is 4.6 for Pt/C and 4.5 for Pt-Cu/C. Both values are close to each other and (within the literature scatter for oxygen concentration and diffusion coefficient values) in line with most reports in literature [26,27,47]. As a result the oxygen reduction follows the $4e^-$ pathway on the Pt surface of the Pt/C as well as the Pt-Cu/C bimetallic catalyst.

In order to asses the activity of the transmetalation catalyst compared to the commercial Pt catalyst the kinetic currents are calculated at low overpotentials, relevant to fuel cell catalysts. Koutechý–Levich plots of Pt/C (Fig. 8) and Pt-Cu/C (Fig. 9) are calculated at 0.8 V and 0.85 V. The minimum correlation coefficient obtained in all measurements is 0.9662. From the intercept of the Koutechý–Levich plots at these potentials the kinetic current (i_k) is calculated. This value has to be correlated with the measured EASA in order to obtain the intrinsic kinetic current density ($j_{k,easa}$). As discussed earlier, the catalyst amount is a main contribution to FC capital costs and therefore also mass normalised kinetic currents will be calculated here. These values are shown in Table 3.

At first sight a clear difference can be seen between the 2 investigated catalysts. Pt-Cu/C has an I_k of 0.21 mA at 0.8 V compared to 0.18 mA for Pt/C. The difference in kinetic current is even higher at 0.85 V with a 19% increase. Conclusions for these values have to be carefully drawn because they do not reveal any intrinsic activity of the catalyst material.

Using the EASA corrected current density (Table 3) as an indication of intrinsic activity, the catalyst ranking is the same as before. However the Pt-Cu/C catalyst now shows even larger rise in activity of 51% and 56% at 0.8 V and 0.85 V respectively. Even though the same mass amount of Pt for every catalyst is applied at the electrode, less of this material is available at the electrode/electrolyte interface for Pt-Cu/C. The mass corrected current density $j_{k,Pt\ mass}$ reaches sufficiently high values for practical fuel cell catalysts. At 0.8 V 1.25E4 mA g^{-1} Pt is measured for Pt/C and 1.44E4 mA g^{-1} Pt for Pt-Cu/C.

Several effects have been attributed to the increased activity in core–shell catalysts. These can be grouped in two main categories: the “ligand effect”-modification of Pt electronic properties by the core metal [48] and the “lattice effect”—mechanism [49]. The former is illustrated by the addition of Cu, Fe, Co, and Ni to Pt which, according to density functional theory should cause a down-shift of the d-band centre of Pt resulting in facilitated oxygen electroreduction [30,50]. In the lattice effect the second metal disrupts the continuity of the Pt lattice resulting in a favourable Pt–Pt bond distance for oxygen adsorption and dissociation [30,20]. Improvements compared to conventional Pt catalysts have also

Table 3
ORR activity of Pt/c and Pt-Cu/C catalysts; the kinetic currents (I_k) are measured at 0.8 V and 0.85 V vs RHE. Normalisation is done using active surface area (j_k, EASA) and Pt mass amount (j_k, m Pt).

E (V vs. RHE)	I_k (mA)		$j_{k,EASA}$ (mA g Pt/m^2 Pt)		$j_{k,Pt\ mass}$ (mA g^{-}1 Pt)	
	Pt-Cu/C	Pt/C	Pt-Cu/C	Pt/C	Pt-Cu/C	Pt/C
0.8	0.21	0.18	6.26E−3	4.14E−3	1.44E4	1.25E4
0.85	0.11	0.09	3.29E−3	2.11E−3	7.59E3	6.37E3

been attributed due to the reduced adsorption of oxygenated spectator species (e.g. OH^-) [18]. The observed gain in activity of the transmetalation catalyst with respect to a commercial Pt FC catalyst indicates that one of the former mechanisms is at play. Since the activity enhancement in a previous study [28] has been shown to depend on the type of alloyed metal, the ligand effect is believed to have the largest contribution. Also, the increase in ORR activity observed for this nanoparticle catalyst with a Pt/Cu atomic ratio of 5 contrasts the behaviour of the particulate catalyst (of a Pt/Cu ratio of 2–3 [30]) produced in [28] where no such effect was observed. This points to the paramount effect that particle morphology and composition plays in this type of bimetallic catalysts with respect to their catalytic activity for a particular reaction.

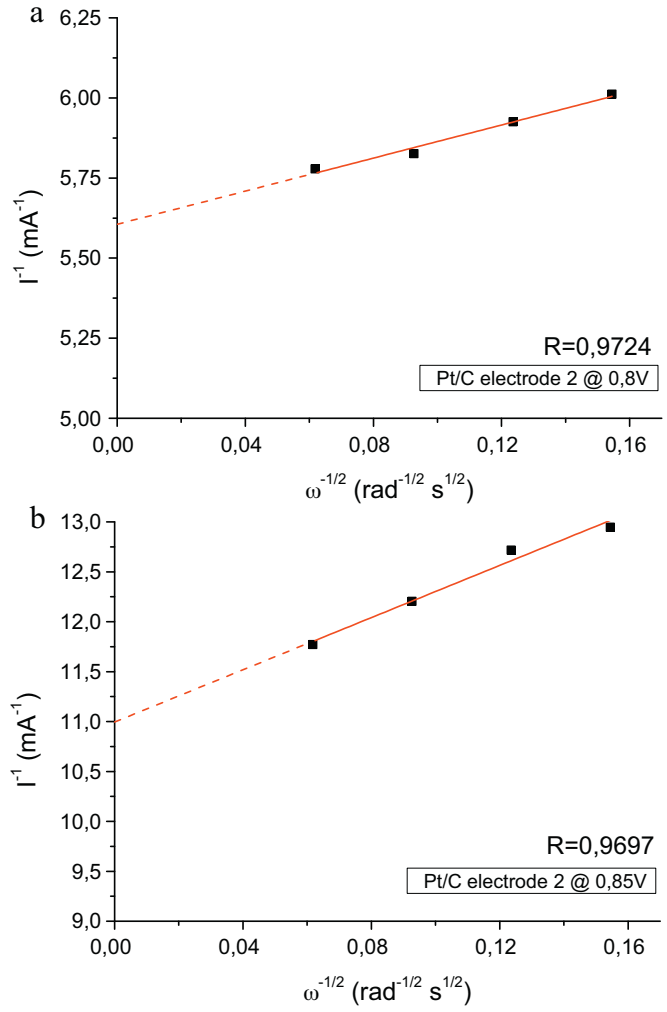

Fig. 8. Koutechý–Levich plots of the Pt/C commercial catalyst at 0.8 V (a) and 0.85 V (b).

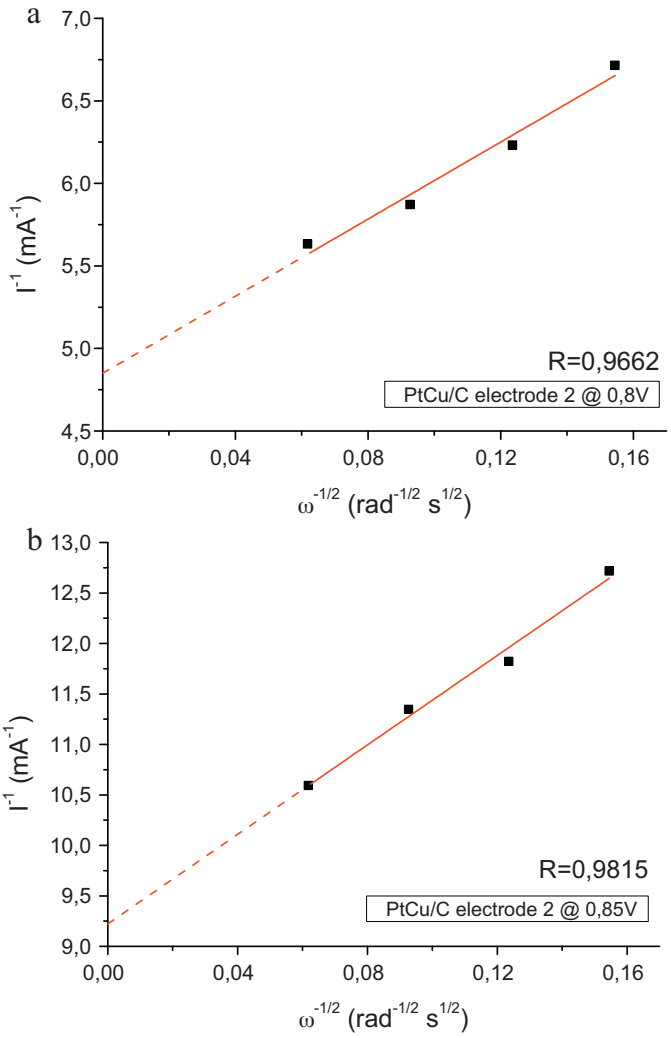

Fig. 9. Koutechý–Levich plots of the Pt-Cu/C catalyst at 0.8 V (a) and 0.85 V (b).

4. Conclusions

Bimetallic Pt-Cu/C catalyst powders, supported on fuel cell technology high surface area carbon supports, have been prepared by a two-step chemical process at room temperature. XRD and XPS experiments confirmed partial alloying of Pt and Cu, whereas cyclic voltammetry in sulfuric acid showed an indication to the presence of a Pt-rich shell. EDS analysis of the commercial Pt/C and the Pt-Cu/C catalyst indicated a 20 wt.% Pt content in the commercial catalyst and 22.7 wt.% in Pt-Cu/C, i.e. the Pt loading of both catalysts is comparable.

The calculated electrochemical active surface area (EASA) values show only small variations within the same type of catalyst. However, a significant difference was found between the two catalysts. The EASA of the Pt-Cu/C nano-structured catalyst was lower than that of the commercial catalyst, probably due to a larger particle

size (3.9 nm compared to 1–2 nm) and the tendency for the formation of aggregates as illustrated by TEM micrographs. In contrast the commercial Pt/C appears to be well dispersed.

The catalytic activity towards the oxygen reduction reaction for the Pt-Cu/C catalyst has been determined using linear sweep voltammetry in combination with a rotating disc electrode. This setup allowed for the calculation of the kinetic current and, in combination with the EASA, the kinetic current density. Results show that the Pt-Cu/C nano-structured catalysts have a 51% higher EASA based catalytic activity at 0.8 V vs RHE compared to the tested commercial catalyst. Even more, at 0.85 V vs RHE the Pt(Cu)/C nano-structured catalyst reaches an even higher (56%) increase in EASA based activity and a moderate (19%) increase in mass-based activity. The "ligand effect"-modification of the Cu core metal is believed to have the largest contribution towards the specific activity enhancement.

Finally, taking into account the results in a previous study [33] the Pt-Cu ratio can be reduced without a significant effect on methanol oxidation reaction (MOR) activity. Depending on particle morphology the same could hold for the ORR activity. This is a strong motivation for further study, aiming at the optimisation of the Pt/Cu ratio for ORR, possibly resulting in less expensive, practically usable Pt-Cu/C core–shell catalysts.

References

[1] S. Srinivasan, Fuel Cells: From Fundamentals to Applications, Springer Science, New York, 2006.
[2] T.E. Lipman, J.L. Edwards, D.M. Kammen, Energy Policy 32 (2004) 101–125.
[3] J.K. Norskov, J. Rossmeisl, A. Logadottir, L. Lindqvist, J.R. Kitchin, T. Bligaard, H. Jonsson, The Journal of Physical Chemistry B 108 (2004) 17886–17892.
[4] P. Mani, R. Srivastava, P. Strasser, Journal of Physical Chemistry C 112 (2008) 2770–2778.
[5] M. Jeon, P. McGinn, Journal of Power Sources 196 (2011) 1127–1131.
[6] R. Yang, J. Leisch, P. Strasser, M.F. Toney, Chemistry of Materials 22 (2010) 4712–4720.
[7] H. Zhu, X. Li, F. Wang, International Journal of Hydrogen Energy 36 (2011) 9151–9154.
[8] E. Antolini, S. Zignani, S. Santos, E. Gonzalez, Electrochimica Acta 56 (2011) 2299–2305.
[9] G. Wu, K.L. More, C.M. Johnston, P. Zelenay, Science (New York, NY) 332 (2011) 443–447.
[10] R. Liu, D. Wu, X. Feng, K. Müllen, Angewandte Chemie (International ed. in English) 49 (2010) 2565–2569.
[11] T.S. Olson, S. Pylypenko, P. Atanassov, K. Asazawa, K. Yamada, H. Tanaka, Journal of Physical Chemistry 114 (2010) 5049–5059.
[12] M. Min, J. Cho, K. Cho, H. Kim, Electrochimica Acta 45 (2000) 4211–4217, 3rd Electrocatalysis Meeting (ECS 99), Portoroz, Slovenia, 1999.
[13] S. Koh, P. Strasser, Journal of the American Chemical Society 129 (2007) 12624–12625.
[14] S. Koh, J. Leisch, M.F. Toney, P. Strasser, Journal of Physical Chemistry C 111 (2007) 3744–3752.
[15] S. Chen, W. Sheng, N. Yabuuchi, P.J. Ferreira, L.F. Allard, Y. Shao-Horn, Journal of Physical Chemistry C 113 (2009) 1109–1125.
[16] C. Wang, G. Wang, D. van der Vliet, K.-C. Chang, N.M. Markovic, V.R. Stamenkovic, Physical Chemistry Chemical Physics 12 (2010) 6933–6939.
[17] Z. Wei, Y. Feng, L. Li, M. Liao, Y. Fu, C. Sun, Z. Shao, P. Shen, Journal of Power Sources 180 (2008) 84–91.
[18] C. Wang, M. Chi, D. Li, D. Strmcnik, D. van der Vliet, G. Wang, V. Komanicky, K.-C. Chang, A.P. Paulikas, D. Tripkovic, J. Pearson, K.L. More, N.M. Markovic, V.R. Stamenkovic, Journal of the American Chemical Society 133 (2011) 14396–14403.
[19] G. Zhang, Z. Shao, W. Lu, F. Xie, H. Xiao, X. Qin, B. Yi, Applied Catalysis B: Environmental 132–133 (2013) 183–194.
[20] a. Sarkar, a. Manthiram, Journal of Physical Chemistry C 114 (2010) 4725–4732.
[21] T. Shibata, B. Bunker, Z. Zhang, D. Meisel, C. Vardeman, J. Gezelter, Journal of the American Chemical Society 124 (2002) 11989–11996.
[22] R. Adzic, J. Zhang, K. Sasaki, M. Vukmirovic, M. Shao, J. Wang, A. Nilekar, M. Mavrikakis, J. Valerio, F. Uribe, Topics in Catalysis 46 (2007) 249–262.
[23] S. Brankovic, J. Wang, R. Adzic, Surface Science 474 (2001) L173.
[24] S. Brankovic, J. McBreen, R. Adzic, Journal of Electroanalytical Chemistry 503 (2001) 99–101.
[25] S. Brankovic, J. McBreen, R. Adzic, Surface Science 479 (2001) L363.
[26] M. Van Brussel, G. Kokkidinis, I. Vandendael, C. Buess-Herman, Electrochemistry Communications 4 (2002) 808.
[27] M. Van Brussel, G. Kokkidinis, A. Hubin, C. Buess-Herman, Electrochimica Acta 48 (2003) 3909.
[28] A. Tegou, S. Papadimitriou, S. Armyanov, E. Valova, G. Kokkinidis, S. Sotiropoulos, Journal of Electroanalytical Chemistry 623 (2008) 187–196.
[29] A. Tegou, S. Papadimitriou, G. Kokkinidis, S. Sotiropoulos, Journal of Solid State Electrochemistry 14 (2009) 175–184.
[30] S. Papadimitriou, S. Armyanov, E. Valova, A. Hubin, O. Steenhaut, E. Pavlidou, G. Kokkinidis, S. Sotiropoulos, Journal of Physical Chemistry C 114 (2010) 5217–5223.
[31] B.I. Podlovchenko, T.D. Gladysheva, a.Y. Filatov, L.V. Yashina, Russian Journal of Electrochemistry 46 (2010) 1189–1197.
[32] C. Xu, Y. Liu, J. Wang, H. Geng, H. Qiu, ACS Applied Materials & Interfaces 3 (2011) 4626–4632.
[33] I. Mintsouli, J. Georgieva, S. Armyanov, E. Valova, G. Adveev, A. Hubin, O. Steenhaut, J. Dille, D. Tsiplakides, S. Balemenou, S. Sotiropoulos, Applied Catalysis B Environmental 136–137 (2013) 160–167.
[34] H. Lang, S. Maldonado, K.J. Stevenson, B.D. Chandler, Journal of the American Chemical Society 126 (2004) 12949–12956.
[35] Y. Ando, K. Sasaki, R. Adzic, Electrochemistry Communications 11 (2009) 1135–1138.
[36] S. Tanuma, C. Powel, D. Penn, Surface and Interface Analysis 17 (1991) 911–926.
[37] D. Baer, M. Engelhard, Journal of Electron Spectroscopy and Related Phenomena 178–179 (2010) 415–432.
[38] J. Armstrong, P. Buseck, Analytical Chemistry 47 (1975) 2178.
[39] N.M. Markovic, P.N.J. Ross, Surface Science Reports 45 (2002) 117–229.
[40] H. Duncan, A. Lasia, Electrochimica Acta 52 (2007) 6195–6205.
[41] M. Odgaard, E.M. Skou, Solid State Ionics 145 (2001) 31–35.
[42] D. Stevens, J. Dahn, Journal of The Electrochemical Society 150 (2003) A770–A775.
[43] S. Machado, A.G.E.R. Tanaka, Electrochimica Acta 36 (1991) 1325–1331.
[44] M. Wünsche, H. Meyer, R. Schumacher, Electrochimica Acta 40 (1995) 629–635.
[45] D. Pletcher, S. Sotiropoulos, Journal of the Chemical Society, Faraday Transactions 91 (1995) 457–462.
[46] Y. Gochi-Ponce, G. Alonso-Nu nez, N. Alonso-Vante, Electrochemistry Communications 8 (2006) 1487–1491.
[47] J. Qiao, R. Lin, B. Li, J. Ma, J. Liu, Electrochimica Acta 55 (2010) 8490–8497.
[48] M. Janssen, J. Moolhuysen, Journal of Catalysis 46 (1977) 289–296.
[49] M. Watanabe, S. Motoo, Journal of Electroanalytical Chemistry 60 (1975) 275–283.
[50] J. Greeley, M. Mavrikakis, Catalysis Today 111 (2006) 52–58.